ADVANCED MATERIALS

DOI: 10.1002/adma.200600258

Evaporation-Induced Self-Assembly (EISA) at Its Limit: Ultrathin, Crystalline Patterns by Templating of Micellar Monolayers**

By *Torsten Brezesinski*,* *Matthijs Groenewolt*,* *Alain Gibaud*, *Nicola Pinna*, *Markus Antonietti*, and *Bernd M. Smarsly**

Patterning of surfaces at the nanoscale is important in many fields of application, e.g., for electronic devices, storage media, and as a starting base for the generation of more complex structures. To exemplify the latter subject, it has been shown that a periodic surface structure with periodicity of surface energy and topology allows for the alignment of liquid crystals[1] or the consecutive construction of channels or pillars being vertically aligned with respect to the substrate,[2] thus making the application of strong external fields redundant.[3,4] Structures in the range of 45–300 nm are predominantly fabricated by either optical- or electron-beam lithography. To reach the sub-45 nm range, self-assembled block-copolymer mesophases are employed as templates within lithographic processes. For instance, Adamson and co-workers reported on the use of block copolymers in a lithography etching process to generate dense periodic arrays of holes and dots in a silicon nitride coated silicon wafer.[5] However, this process deals only with the structuring of a given surface, i.e., the physical properties of the final material are limited by the choice of the starting material and the restrictions of lithography.

[*] Dr. T. Brezesinski, Dr. B. M. Smarsly, Prof. M. Antonietti
Max Planck Institute of Colloids and Interfaces
Research Campus Golm
Am Mühlenberg 1, 14476 Potsdam-Golm (Germany)
E-mail: Torsten.Brezesinski@mpikg.mpg.de;
Smarsly@mpikg.mpg.de
Dr. M. Groenewolt
BASF Coatings AG, CT/R-A301
48165 Münster (Germany)
E-mail: Matthijs.Groenewolt@mpikg.mpg.de
Prof. A. Gibaud
Laboratoire de Physique de L'Etat Condensé, UMR CNRS 6087
Université du Maine
72085 Le Mans, Cedex 09 (France)
Dr. N. Pinna
Departamento de Química, CICECO, Universidade de Aveiro
3810-193 Aveiro (Portugal)
Dr. N. Pinna
Max-Planck-Institute of Microstructure Physics
Weinberg 2, 06120 Halle/Saale (Germany)

[**] We thank Dr. Helmut Schlaad for providing the block copolymer and Dr. Arne Thomas for the technical help throughout EM studies. Further on, we thank Dr. Peter Werner from the MPI of Microstructure Physics for assistance with the high-resolution electron microscopy and for fruitful discussions. The Max Planck Society is acknowledged for financial support. In addition, this work was supported by the French ACI 2004 under the acronym "Autofymehypodir". Supporting Information is available online from Wiley InterScience or from the author.

Herein, we present a straightforward approach towards a whole range of ultrathin, mesostructured metal oxide layers by sol–gel processing via a modified evaporation-induced self-assembly (EISA) approach introduced by Ogawa et al. and Brinker et al. several years ago.[6] EISA usually provides mesostructured films with a thickness of 50–1000 nm, which therefore consist of several stacked layers (multilayers of micellar aggregates).[7] However, it is challenging to use this well-established procedure to generate corresponding ultrathin films with ordered mesoporosity, although it is usually assumed that such fine control can only be achieved by Langmuir–Blodgett (LB) techniques. Kunitake and co-workers reported the successful preparation of ultrathin, self-supporting films of different oxides by sequential sol–gel processing using polymer underlayers and spin-coating, but the porosity was disordered and the metal oxides amorphous.[8]

In the present study, it is shown that a modified EISA procedure allows for the preparation of crack-free, ultrathin, crystalline metal oxide films with highly ordered in-plane mesostructure and a tunable film thickness on the scale of only several nanometers, even achieving the sequential formation of mesostructured metal oxides with exactly one micellar monolayer in height. Different structures (e.g., circular pores or line patterns) of the final surface layer material can be simply adjusted by varying the assembly structure of the template, and by using sufficiently small templates, the periodicity of the patterns can be downsized to about 4–5 nm. In addition, the structure is instantaneously generated on macroscopic length scales (i.e., not serial/slow). This has been beyond the reach of common lithography techniques to date. Furthermore, in contrast to physical methods such as molecular-beam epitaxy, pulsed laser deposition, and chemical vapor deposition, which are often used in combination with lithography and are known to suffer from elaborate preparation techniques, the present sol–gel approach also allows one to address more complex metal oxides (e.g., $BaTiO_3$) by the ease of "beaker" chemistry and liquid-coating processing.

For the generation of ultrathin, mesoporous metal oxide layers with periodicities in two dimensions and one dimension, respectively, we used two different types of structure-directing agents, namely a novel block copolymer of the "KLE" family (poly(ethylene-*co*-butylene)-*block*-poly(ethylene oxide)),[9] which has already enabled the synthesis of various mesoporous, crystalline metal oxide thin films (e.g., CeO_2,[10] TiO_2,[11] γ-Al_2O_3,[12] FeO_x,[13] $SrTiO_3$[14]) and the well-known classical nonionic surfactant "Brij 58".[15] The thickness of

WILEY InterScience DISCOVER SOMETHING GREAT
© 2006 WILEY-VCH Verlag GmbH & Co. KGaA, Weinheim

patterned surfaces was thereby mainly controlled by two parameters, the withdrawal speed during dip-coating and the initial concentration of the used sol, in agreement with the studies of Brinker and co-workers.[16] Apparently, the combination of experimental conditions of the LB-film generation, i.e., highly dilute systems, with the EISA process, i.e., fast evaporation of the solvent(s) used, provides facilities for the sequential formation of metal oxide layers with periodic 1D and 2D mesoporosity. Such LB-like monolayers can be deposited onto arbitrary, flat substrates (e.g., silicon wafer or glass), leading to a reduction of the 3D spherical and hexagonal bulk morphologies obtained by conventional EISA techniques, into flat 2D arrays of hexagonally/rectangularly arranged circular holes and 1D-aligned channels with cylinder axes oriented parallel to the substrate plane.

Figure 1 shows two different morphologies of micellar monolayers, transferred into crystalline metal oxide replicas (here WO_3 and CeO_2). The transmission electron microscopy (TEM) images already demonstrate the high quality of the ultrathin textures over micrometer-sized areas together with the absence of cracks and larger structural defects. Interestingly, a

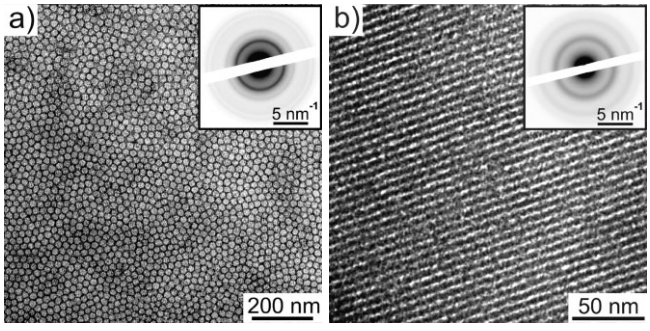

Figure 1. Transmission electron microscopy images showing two different types of ordered monolayer morphologies of mesostructured metal oxide films after crystallization and removal of the template. a) A "KLE"-templated WO_3 layer containing pores with a local hexagonal order and b) a "Brij 58"-templated CeO_2 film with 1D-aligned channels. Insets show selected area electron diffraction patterns of the same zones, revealing diffraction rings characteristic of polycrystalline structures.

lateral mesopore diameter of ca. 20–25 nm was obtained for the different "KLE"-templated films, which was substantially larger compared to the pore size in 3D-mesoporous films (ca. 10–15 nm) prepared with the same polymer template. This finding indicates that surface effects significantly modify or deform the block-copolymer micelles, in the extreme creating circular, "dropletlike" admicelles.[17] However, "Brij 58"-derived line patterns (cylindrical micelles) revealed an in-plane lattice parameter of ca. 4–6 nm (depending on the heat treatment), in line with corresponding 3D-mesoporous films.[15]

Selected area electron diffraction (SAED) was used to verify the crystallinity of the walls in between the pores or channels. The SAED patterns (Fig. 1a and b (insets) and Fig. 2d) display diffraction rings characteristic of polycrystalline structures, in which the nanocrystallites are randomly oriented

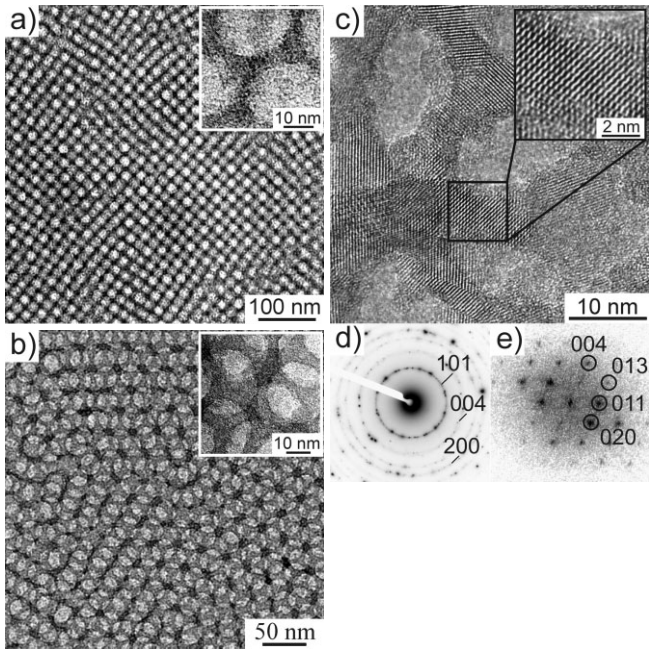

Figure 2. Electron microscopy study of "KLE"-templated TiO_2 films after calcination at 550 °C. TEM images of ultrathin TiO_2 coatings featuring either a) a monolayer or b) a bilayer of highly ordered mesopores arranged on a 2D cubic lattice (insets are magnifications). The apparent pore sizes (in-plane) are 22–24 nm for both the mono- and bilayer. In both cases the pore-to-pore distance (along the [10] direction) is ca. 26–28 nm. c) High-resolution TEM image of the mesostructure (corresponding to (b)), showing the crystalline nanoparticles building up the framework (inset shows characteristic lattice planes of a single TiO_2 nanocrystal). d) SAED pattern of the same zone. e) Power spectrum (Fourier transform of the inset of (c)) revealing characteristic reflections of an anatase single nanocrystal oriented along the [100] direction.

with respect to one another. The calculated *d*-spacings are in agreement with the monoclinic crystal modification of WO_3 (No. 43-1035, Joint Committee for Powder Diffraction Studies, JCPDS), synthetic cerianite (No. 43-1002) and anatase (No. 21-1272). Besides SAED, high-resolution TEM (HRTEM) was used to visualize the crystalline character of the mesoporous framework, which is exemplified for a TiO_2 film, corresponding to Figure 2b, and a CeO_2 film (Supporting Information), both with circular pore structures. Figure 2c shows that indeed the pore walls are fully composed of randomly oriented nanocrystallites, the size of which was estimated to be ca. 6–10 nm. Significant amorphous fractions in the metal oxide frameworks could practically be excluded. Note that most of the oxide materials exhibit their specific physicochemical properties only in the crystalline state.

In this context, we want to emphasize again that we were able to adjust the film thickness on the nanoscale with a rather high degree of control, as shown for TiO_2 films with either a monolayer or bilayer of highly ordered mesopores (Fig. 2). Such basic constructions of spherical dense packing motifs have up to now only been achieved by applying almost monodisperse, colloidal particles in combination with special deposition processes, however on length scales being one order

 © 2006 WILEY-VCH Verlag GmbH & Co. KGaA, Weinheim

ADVANCED MATERIALS

of magnitude larger.[18] The formation of "quantized" numbers of mesostructured layers can thereby be explained as follows: Since we are dealing with a dense packing motif of spheres, the boundary between two micellar layers can be considered as a gliding plane, in analogy to metals with cubic lattices. As the change of density is minimal along such a plane, the critical shear stress to initiate the moving of spheres (micelles) is very low compared to the one within a layer.[19] For this reason, we observed solely discrete layers in the final structure, e.g., mono- or bilayers, but not templated micellar layers with some additional spheres (micelles, pores) on top of them. Although the 2D rectangular arrangement of spheres does not have 3D periodicity, the packing seen for the TiO_2 bilayer can formally be attributed to the packing of pores of a bcc (body-centered cubic) structure in the [110] orientation, which is in accordance with the structure recently observed for the corresponding 3D-mesoporous films. No significant differences (1–3 nm at maximum) in the lateral pore size were found for mono- and bilayer films. In the same way, metal oxides forming face-centered cubic (fcc) structures of spherical mesopores (such as Al_2O_3, SiO_2, and MoO_3) show 2D hexagonal monolayer pore arrangements. Such patterns are also in line with the [111] orientation seen for the thicker films (see Supporting Information), which is the packing with the highest structural density.

Beside electron microscopy, the mesostructures were also studied by means of X-ray reflectivity (XRR), which is exemplified for a TiO_2 film, featuring a monolayer of mesopores. The XRR data, shown in Figure 3, display a series of maxima and minima, attributable to the form factor of spherical mesopores. These data could be successfully fitted based on two models. First, the analysis was performed using the matrix technique, which had already been applied to cylindrical mesostructures.[20] In essence, the model is based on two alternating stacked layers on a silicon substrate. From this approach, a film thickness of ca. 13–14 nm was obtained. The corresponding electron density profile (Fig. 3b) revealed a porous layer of ca. 4–5 nm, which is attributable to the mesopores. Since this layer model does not take into account the shape of pores, the data were also evaluated in terms of small-angle X-ray scattering (SAXS) in symmetric reflection. The applied model uses scattering functions described in the literature[21] and was able to fit the oscillations as a result of a well-defined form factor of spheres. The analysis provided an average pore height of ca. 6 nm and a layer thickness of ca. 17–18 nm, being in good agreement with the XRR results. In conclusion, both analyses confirmed the formation of a monolayer of well-defined, "disklike" mesopores embedded in a crystalline TiO_2 matrix.

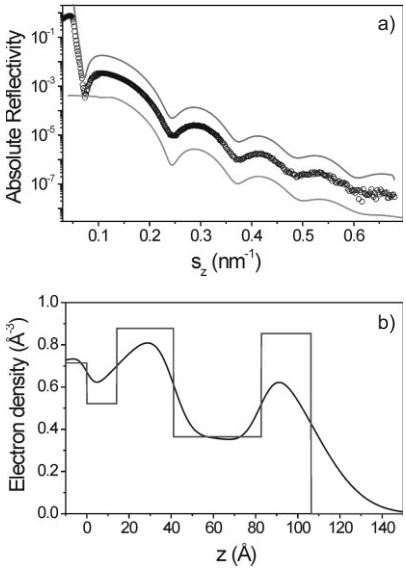

Figure 3. XRR analysis of a "KLE"-templated TiO_2 film, featuring a monolayer of well-ordered, "disklike" mesopores. a) Curve fitting using either the matrix technique (top curve) or an evaluation in terms of SAXS in symmetric reflection (bottom curve). b) Calculated electron density profile (using the matrix technique). The arrow indicates the electron density of the silicon substrate.

Finally, various calcination experiments were performed to study the influence of the thin layer confinement on the thermal stability of the ultrathin films with well-ordered in-plane mesostructure. The obtained data featured several interesting features. First, a time-consuming pretreatment of films at moderate temperatures is not required to solidify or stabilize the mesostructured, amorphous network prior to crystallization, as recently reported for the generation of diverse mesoporous, crystalline films with intricate sol–gel behavior.[10,12,13,22] Second, at least for TiO_2, the layers possess a better thermal stability than corresponding 3D-mesoporous films synthesized with the same polymer template, i.e., the mesostructural collapse due to mass transport in the pore walls takes place at higher temperatures (ca. 750 °C compared to ca. 700 °C for 3D-mesoporous TiO_2 films), which can be explained by the strong mesoscopic confinement and interaction with the surface, hindering diffuse sintering of the nanoparticles. Further experiments will clarify whether this effect can be generalized.

To conclude, it was demonstrated that a wide variety of metal oxide precursors can be used for the generation of ultrathin, highly crystalline, binary, and even more complex metal oxide layers (e.g., indium tin oxide, FeO_x, $SrTiO_3$) with periodic 1D and 2D mesoporosity. With the shown modified EISA process, the thickness of films can be adjusted on the scale of only several nanometers by the run-off of films stabilizing specifically monolayers, bilayers, etc. with high lateral perfection. These films were then easily transformed into their crystalline counterparts by straightforward calcination without the necessity of pretreatment steps. For this reason, the present approach can be exploited for the generation of periodic surface structures featuring a well-defined in-plane mesostructure and a high crystallinity at the same time.

Moreover, the investigations of ultrathin layers provided novel, interesting insights into the behavior of block copolymers close to interfaces. The most striking feature is the significantly increased lateral diameter of the mesopores in comparison to 3D-mesoporous films of the same material. Since this phenomenon is combined with a compression perpendicular to the surface, we assume that the spherical micelles are

 © 2006 WILEY-VCH Verlag GmbH & Co. KGaA, Weinheim

flattened out towards "disklike" objects, presumably by the interaction of the polar poly(ethylene oxide) corona chains with the polar substrate.

Current work is related to combine the present strategy with the approach of Miyata et al. to generate ultrathin, single-crystalline domains, which are indispensable for technological applications.[23] In addition, the patterned surfaces are used to analyze the influence of nanoscopic surface roughness on wetting properties.

Experimental

The diblock copolymer ($H(CH_2CH_2CH_2(CH)CH_2CH_3)_{89}(OCH_2CH_2)_{79}OH$, "KLE") used in this study was synthesized in our labs. The synthetic procedure is shown elsewhere [8]. Other chemicals were purchased from Aldrich and used without further purification.

Synthesis of Ultrathin, Mesoporous Metal Oxide Films: In a typical synthesis, the structure-directing agent was dissolved in 3 mL EtOH and added to a solution containing the metal oxide precursor in a mixture of 1 mL tetrahydrofuran, 3 mL ethanol (EtOH), and some water (depending on the metal oxide system, detailed recipes are given in Table 1). Afterwards, the resulting isotropic sol was stirred for 1 h prior to chemical solution deposition. Ultrathin films were deposited by dip-coating RCA-cleaned [24], flat substrates such as silicon and glass (gold-coated copper grids were used for electron microscopy studies) at a constant relative humidity (20–40 %). Micellar monolayers were obtained at a withdrawal rate of 0.5 mm s^{-1}, whereas bilayers were formed at 1.5 mm s^{-1}. Finally crystallization was induced by straightforward heating with a ramp of 5–10 °C min^{-1} in air.

Table 1. Detailed recipes for the syntheses of various ultrathin, mesoporous metal oxide films. The "KLE" polymer template was used to generate spherical micelles, whereas "Brij58" generated cylindrical micelles.

Metal oxide system	Precursor [mg]	Water [mg]	Structure-directing agent [mg]	Crystallization temperature [°C]
"KLE"-templated WO_3	WCl_6 70	–	17	500
"KLE"-templated TiO_2	$TiCl_4$ 80	60	13	500–520
"KLE"-templated MoO_3	$MoCl_5$ 100	–	20	450
"KLE"-templated CeO_2	$CeCl_3{\cdot}7H_2O$ 70	50	14	280–300
"Brij58"-templated CeO_2	$CeCl_3{\cdot}7H_2O$ 70	50	30–35	300

Characterization: TEM images were taken with a Zeiss EM 912Ω at an acceleration voltage of 120 kV, whereas a Jeol 4010 operated at 400 kV equipped with a LaB_6 cathode was used for HRTEM. XRR was carried out on a Philips reflectometer at a wavelength of 1.54 Å.

Received: February 8, 2006
Final version: April 6, 2006
Published online: August 8, 2006

[1] a) C. Weder, C. Sarwa, C. Bastiaansen, P. Smith, *Adv. Mater.* **1997**, *9*, 1035. b) N. Stutzmann, T. A. Tervoort, D. J. Broer, H. Sirringhaus, R. H. Friend, P. Smith, *Adv. Funct. Mater.* **2002**, *12*, 105.

[2] a) D. Y. Ryu, K. Shin, E. Drockenmuller, C. J. Hawker, T. P. Russell, *Science* **2005**, *308*, 236. b) C. J. Hawker, T. P. Russell, *MRS Bull.* **2005**, *30*, 952. c) P. Mansky, Y. Liu, E. Huang, T. P. Russell, C. Hawker, *Science* **1997**, *275*, 1458.

[3] S. H. Tolbert, A. Firouzi, G. D. Stucky, B. F. Chmelka, *Science* **1997**, *278*, 265.

[4] a) T. L. Morkved, M. Lu, A. M. Urbas, E. E. Ehrichs, H. M. Jaeger, P. Mansky, T. P. Russell, *Science* **1996**, *273*, 931. b) T. Thurn-Albrecht, J. Schotter, C. A. Kastle, N. Emley, T. Shibauchi, L. Krusin-Elbaum, K. Guarini, C. T. Black, M. T. Tuominen, T. P. Russell, *Science* **2000**, *290*, 2126.

[5] M. Park, C. Harrison, P. M. Chaikin, R. A. Register, D. H. Adamson, *Science* **1997**, *276*, 1401.

[6] a) M. Ogawa, *Langmuir* **1997**, *13*, 1853. b) C. J. Brinker, Y. F. Lu, A. Sellinger, H. Y. Fan, *Adv. Mater.* **1999**, *11*, 579. c) C. J. Brinker, *MRS Bull.* **2004**, *29*, 631.

[7] a) P. D. Yang, D. Y. Zhao, D. I. Margolese, B. F. Chmelka, G. D. Stucky, *Nature* **1998**, *396*, 152. b) L. Nicole, C. Boissière, D. Grosso, A. Quach, C. Sanchez, *J. Mater. Chem.* **2005**, *15*, 3598.

[8] a) M. Hashizume, T. Kunitake, *Langmuir* **2003**, *19*, 10172. b) J. Huang, I. Ichinose, T. Kunitake, A. Nakao, *Langmuir* **2002**, *18*, 9048.

[9] A. Thomas, H. Schlaad, B. Smarsly, M. Antonietti, *Langmuir* **2003**, *19*, 4455.

[10] a) T. Brezesinski, B. Smarsly, M. Groenewolt, M. Antonietti, D. Grosso, C. Boissière, C. Sanchez, *Stud. Surf. Sci. Catal.* **2005**, *156*, 243. b) T. Brezesinski, M. Groenewolt, N. Pinna, M. Antonietti, B. Smarsly, *New J. Chem.* **2005**, *29*, 237.

[11] B. Smarsly, D. Grosso, T. Brezesinski, N. Pinna, C. Boissière, M. Antonietti, C. Sanchez, *Chem. Mater.* **2004**, *16*, 2948.

[12] M. Kuemmel, D. Grosso, C. Boissière, B. Smarsly, T. Brezesinski, P. A. Albouy, H. Amenitsch, C. Sanchez, *Angew. Chem. Int. Ed.* **2005**, *44*, 4589.

[13] T. Brezesinski, M. Groenewolt, M. Antonietti, B. Smarsly, *Angew. Chem. Int. Ed.* **2006**, *45*, 781.

[14] D. Grosso, C. Boissière, B. Smarsly, T. Brezesinski, N. Pinna, P. A. Albouy, H. Amenitsch, M. Antonietti, C. Sanchez, *Nat. Mater.* **2004**, *3*, 787.

[15] B. Smarsly, A. Gibaud, W. Ruland, D. Sturmayr, C. J. Brinker, *Langmuir* **2005**, *21*, 3858.

[16] a) C. J. Brinker, G. C. Frye, A. J. Hurd, C. S. Ashley, *Thin Solid Films* **1991**, *201*, 97. b) A. Gibaud, D. Grosso, B. Smarsly, A. Baptiste, J. F. Bardeau, F. Babonneau, D. A. Doshi, Z. Chen, C. J. Brinker, C. Sanchez, *J. Phys. Chem. B* **2003**, *107*, 6114.

[17] A. D. W. Carswell, E. A. O'Rear, B. P. Grady, *J. Am. Chem. Soc.* **2003**, *125*, 14793.

[18] a) A. S. Dimitrov, K. Nagayama, *Langmuir* **1996**, *12*, 1303. b) J. E. G. J. Wijnhoven, W. L. Vos, *Science* **1998**, *281*, 802. c) O. D. Velev, P. M. Tessier, A. M. Lenhoff, E. W. Kaler, *Nature* **1999**, *401*, 548. d) Y. A. Vlasov, X.-Z. Bo, J. C. Sturm, D. J. Norris, *Nature* **2001**, *414*, 289.

[19] a) R. von Klitzing, A. Espert, D. Langevin, *Colloids Surf., A* **2001**, *176*, 109. b) B. Kolaric, W. Jaeger, R. von Klitzing, *J. Phys. Chem. B* **2000**, *104*, 5096.

[20] a) J. F. Bardeau, A. Gourbil, M. Dutreilh-Colas, S. Dourdain, A. Mehdi, A. Gibaud, *Thin Solid Films* **2006**, *495*, 191. b) A. Gibaud, S. Hazra, *Curr. Sci.* **2000**, *78*, 1467.

[21] B. Smarsly, M. Groenewolt, M. Antonietti, *Prog. Colloid Polym. Sci.* **2005**, *130*, 105.

[22] a) V. N. Urade, H. W. Hillhouse, *J. Phys. Chem. B* **2005**, *109*, 10538. b) T. Brezesinski, A. Fischer, K. Iimura, C. Sanchez, D. Grosso, M. Antonietti, B. Smarsly, *Adv. Funct. Mater.*, in press.

[23] a) H. Miyata, K. Kuroda, *Chem. Mater.* **2000**, *12*, 49. b) H. Miyata, T. Suzuki, A. Fukuoka, T. Sawada, M. Watanabe, T. Noma, K. Takada, T. Mukaide, K. Kuroda, *Nat. Mater.* **2004**, *3*, 651.

[24] W. Kern, *RCA Rev.* **1970**, *31*, 187.

 © 2006 WILEY-VCH Verlag GmbH & Co. KGaA, Weinheim